coatings

MDPI

Article

Plasma Enhanced Atomic Layer Deposition of Tantalum (V) Oxide

Pavel Fedorov [1], Denis Nazarov [1,2], Oleg Medvedev [1], Yury Koshtyal [1,3], Aleksander Rumyantsev [1,3], Vladimir Tolmachev [3], Anatoly Popovich [1] and Maxim Yu Maximov [1,*]

[1] Peter the Great Saint-Petersburg Polytechnic University, 195221 Saint Petersburg, Russia; fedorovpavel99@yandex.ru (P.F.); dennazar1@yandex.ru (D.N.); medvedev.os1990@gmail.com (O.M.); yury.koshtyal@gmail.com (Y.K.); rumyantsev.amr@gmail.com (A.R.); director@immet.spbstu.ru (A.P.)
[2] Saint Petersburg State University, 199034 Saint Petersburg, Russia
[3] Ioffe Institute, 194021 Saint Petersburg, Russia; tva@mail.ioffe.ru
* Correspondence: maximspbstu@mail.ru

Abstract: The tantalum oxide thin films are promising materials for various applications: as coatings in optical devices, as dielectric layers for micro and nanoelectronics, and for thin-films solid-state lithium-ion batteries (SSLIBs). This article is dedicated to the Ta-O thin-film system synthesis by the atomic layer deposition (ALD) which allows to deposit high quality films and coatings with excellent uniformity and conformality. Tantalum (V) ethoxide ($Ta(OEt)_5$) and remote oxygen plasma were used as tantalum-containing reagent and oxidizing co-reagent, respectively. The influence of deposition parameters (reactor and evaporator temperature, pulse and purge times) on the growth rate were studied. The thickness of the films were measured by spectroscopic ellipsometry, scanning electron microscopy and X-ray reflectometry. The temperature range of the ALD window was 250–300 °C, the growth per cycle was about 0.05 nm/cycle. Different morphology of films deposited on silicon and stainless steel was found. According to the X-ray diffraction data, the as-prepared films were amorphous. But the heat treatment study shows crystallization at 800 °C with the formation of the polycrystalline Ta_2O_5 phase with a rhombic structural type (Pmm2). The results of the X-ray reflectometry show the Ta-O films' density is 7.98 g/cm^3, which is close to the density of crystalline Ta_2O_5 of the rhombic structure (8.18 g/cm^3). The obtained thin films have a low roughness and high uniformity. The chemical composition of the surface and bulk of Ta-O coatings was studied by X-ray photoelectron spectroscopy and energy-dispersive X-ray spectroscopy. Surface of the films contain Ta_2O_5 and some carbon contamination, but the bulk of the films does not contain carbon and any precursor residues. Cyclic voltammetry (CVA) showed that there is no current increase for tantalum (V) oxide in a potential window of 3–4.2 V and has prospects of use as protective coatings for cathode materials of SSLIBs.

Keywords: plasma-enhanced atomic layer deposition; tantalum oxide; thin films; spectroscopic ellipsometry; li-ion batteries; solid-state batteries; LIB's protective coatings

Citation: Fedorov, P.; Nazarov, D.; Medvedev, O.; Koshtyal, Y.; Rumyantsev, A.; Tolmachev, V.; Popovich, A.; Maximov, M.Y. Plasma Enhanced Atomic Layer Deposition of Tantalum (V) Oxide. *Coatings* **2021**, *11*, 1206. https://doi.org/10.3390/coatings11101206

Academic Editors: Octavian Buiu and Alessio Lamperti

Received: 13 August 2021
Accepted: 28 September 2021
Published: 1 October 2021

1. Introduction

Thin films of tantalum oxide are used for antireflection coatings for strongly curved glass lenses [1], as dielectric layers for micro and nanoelectronics [2]. They also have great prospects for solid-state lithium-ion batteries (SSLIB) [2] as a solid-state electrolyte and functional coatings for cathodes.

It is important to use low deposition temperatures to prevent structural and chemical changes in the surface of the coated material while obtaining films for previously mentioned purposes. The ability to cover 3D-oriented surfaces with precise thickness control is also important. All these tasks can be solved by the Atomic Layer Deposition (ALD) [3]. The essence of the method lies in the chemical interaction of reagent vapors with the substrate and subsequent purging with an inert gas. Due to its peculiarities, the method makes

it possible to obtain uniform films and high-quality coatings on surfaces of both flat and bulk three-dimensional substrates. It allows controlling the thickness of the films with a high accuracy, and also provides good reproducibility of the resulting structures characteristics [4].

Both inorganic (TaF_5, $TaCl_5$), and a number of organometallic precursors (TBTEMT, Ta(NtBu)Me(dmaema)$_2$, (t-BuN)(Et$_2$N)$_2$CpTa, TBTMET, TBTDET, TAIMATA, PDMAT, Ta(OEt)$_5$) are used to obtain tantalum oxides by the ALD (Table 1). The metal halide precursors have high vapor pressure are stable, reactive and therefore widely used. But the use such inorganic reagents lead to formation of corrosive byproducts (e.g., HCl) which may cause possible etching of growing film and damage hardware of the ALD tools. Alkylamides such as (t-BuN)(Et$_2$N)$_2$CpTa, TBTEMT, TBTMET, PDMAT have limited thermal stability and low reactivity which can be improved by increasing the ALD temperature, but this can lead to thermal decomposition of the metalorganic precursors. Tantalum (V) ethoxide (Ta(OEt)$_5$) is a liquid with a saturated vapor pressure high enough for ALD processes (6 mm Hg at 190 °C) [5]. The reagent is relatively stable during storage and it does not decompose in the ALD "window" temperature range [6] and can be successful used for the ALD. To date, a number of researchers have shown that both water and oxygen plasma can be successfully used as co-reagents for Ta(OEt)$_5$ (Table 1). However, despite the existence of a number of studies, the features of the growth, structure, composition and morphology of tantalum oxide films using Ta(OEt)$_5$ and remote oxygen plasma have not been studied in detail.

This work is devoted to studying the ALD growth parameters of tantalum (V) oxide thin films using tantalum (V) ethoxide and remote oxygen plasma by different methods. The chemical composition at the surface and in-depth, structure (phase composition, thin films density, roughness), the morphology of Ta-O thin films on the silicon and stainless steel substrates were studied. The electrochemical performance is provided by cyclic voltammetry.

Table 1. Comparative characteristics of the tantalum binary compounds obtaining processes by the ALD method.

Precursor A CAS No	Precursor B	Reagent Temperature °C	Reactor Temperature °C	Substrate	Growth Per Cycle (GPC) nm/cycle	Chemical Compound	Ref.
$Ta(OEt)_5$ 6074-84-6	O_2 plasma	110	220	Si, TiN	0.09	Ta_2O_5	[7]
	O_2 plasma	-	260	Si	0.075	Ta_2O_5	[8]
	H_2O_2	185	300	Si	0.049	Ta_2O_5	[1]
	H_2O	70	200–350	Si	0.040 ± 0.001	Ta_2O_5	[9]
	H_2O	190	225	Si	0.05	Ta_2O_5	[10]
	O_2 plasma, H_2O	-	300	SiO_2, Si	-	Ta_2O_5	[11]
	H_2O	-	250	SiO_2, Si	-	Ta_2O_5	[12]
	H_2, H_2O	-	300	Si, TiN	-	Ta_2O_5	[13]
	H_2	-	300	Si	0.052	Ta_2O_5	[14]
	H_2O	-	250	Si	-	Ta_2O_5	[15]
	O_3	95	300	SiO_2	0.035	Ta_2O_5	[16]
	O_3	160	100–400	TiN/SiO_2	0.095–0.113	Ta_2O_5	[17]
TBTEMT $Ta[N(CH_3)(C_2H_5)]_3[=NC(CH_3)_3]$ 511292-99-2	H_2O	90	210	Al_2O_3, SiO_2	0.051	Ta_2O_5	[18]
	H_2, Ar:H_2	-	150–350	Si	-	TaN	[19]
TaF_5 7783-71-3	H_2, Ar plasma	70	350	-	0.035	TaN	[20]
	Mixed H_2 + Ar + N_2	70	350	SiO_2, Si	0.041	TaN	[21]
TBTMET, TBTDMT, $Ta[N(CH_3)_2]_3[=NC(CH_3)_3]$ 69039-11-8	O_2 plasma	60	250	Si	0.01	Ta_2O_5	[22]
	N_2:H_2, NH_3, O_2	-	300–400	SiO_2, Si	-	Ta_2O_5	[23]
	O_2 plasma	55	300	Si	0.11	Ta_2O_5	[24]
TBTDET, $Ta[N(C_2H_5)_2]_3[=NC(CH_3)_3]$ 169896-41-7	H_2O	100	150–350	Si	0.077	Ta_2O_5	[25]

Table 1. *Cont.*

Precursor A CAS No	Precursor B	Reagent Temperature °C	Reactor Temperature °C	Substrate	Growth Per Cycle (GPC) nm/cycle	Chemical Compound	Ref.
TAIMATA 629654-53-1	N_2+H_2 plasma	60	230	SiO_2, Si(100)	0.13	TaN	[26]
	Ar + H_2	-	300	SiO_2, Si(100), HfO_2	-	TaC, TaN	[27]
	Ar+H_2	70	350	SiO_2, Si	0.09–0.1	TaN	[28]
	H_2	60	230	SiO_2, Si	0.13	TaN, TaC	[29]
	H_2O	-	200	Si	-	TaN	[30]
PDMAT, $Ta[N(CH_3)_2]_5$ 19824-59-0	O_2 plasma	65	100–225	Si(100)	0.08–0.087	Ta_2O_5	[31]
$(t\text{-BuN})(Et_2N)_2CpTa$ 852212-55-6	H_2O	-	200	-	-	Ta_2O_5	[32]
$Ta(NtBu)Me(dmaema)_2$	NH_3 plasma	100–120	200–250	SiO_2, Si	0.062	TaN	[33]
$TaCl_5$ 7721-01-9	H_2O	90	250–450	Si	0.011–0.065	Ta_2O_5	[6]
	H_2:N_2	90	300	Si(001), SiO_2	0.024	TaN	[34]
	H_2:N_2	-	300	Si	0.008–0.01	TaN	[35]
	H_2:N_2	100	100–400	Si(001), SiO_2	0.024	TaN	[36]
	H_2:N_2	110	300	SiO_2	-	TaN	[37]
	Atomic H	100	25–300	SiO_2, Si	0.008	Ta	[38]
	Atomic H	100–120	25–400	Si	0.016–0.16	Ta	[2]
	Atomic H	100	400	Si(001), SiO_2	0.008	Ta	[39]

2. Materials and Methods

$Ta(OEt)_5$ (Sigma Aldrich, 99.98% trace metal basis) was used to obtain tantalum oxide films on a Picosun R-150 set up in the reactor temperature range from 225 to 350 °C. Ta(OEt)5 was stored in a stainless steel bottle (PicohotTM 200, Picosun Oy, Espoo, Finland) and heated during synthesis to 70, 90, 110, 160, and 190 °C. The pulse time was varied from 0.5 s to 2 s, and purge time was changed from 5 s to 15 s. At an inert nitrogen purge, the gas pressure of 8–12 hPa is combined with vacuum pumping. The number of cycles for the samples ranged from 50 to 1000. Remote oxygen plasma was used as a co-reagent (oxidizer). Plasma power was 3000 W, and the frequency was 1.9–3.2 MHz. The total plasma pulse time was 19.5 s. First, Ar purge was carried out for 0.5 s at a flow rate of 40 sccm, Ar and O_2 plasma purge was carried out for 14 s at a flow rate of 90 sccm. And the last part was Ar purge for 5 s at a flow rate flow 40 sccm. Thus, the number of cycles for the samples ranged from 50 to 1000.

Monocrystalline silicon substrates (surface orientation (100), 40 × 40 mm, TelecomSTV Co., Ltd., Zelenograd, Russia) and stainless-steel disks (316SS, 16 mm diameter, Tob New Energy Technology Co., Ltd., Xiamen, China) were used in experiments as substrates for the ALD. Before deposition, the stainless-steel substrates were cleaned in an ultrasonic bath filled with acetone and then deionized water for 5 min.

Spectroscopic ellipsometry (SE) [40,41] was used to determine the thickness of the resulting films and to calculate the growth per cycle (GPC). Ellipsometric measurements were performed with a spectroscopic ellipsometer Ellips-1891 SAG (CNT, Novosibirsk, Russia) at wavelengths in the range λ = 250–900 nm (photon energy E = 1.4–5.0 eV) and light incidence angle φ = 70° relative to the normal to the surface, from an external medium (air). Spectral dependences of both ellipsometric angles ψ and Δ were measured simultaneously. The probe spot diameter was 3 mm. The calculations were carried out using the procedure for finding the model (Supplementary file) coefficients and film thickness using the software supplied with the ellipsometer. The thickness measurement error was ±1 nm.

X-ray reflectometry (XRR) and X-ray diffraction (XRD) studies were performed on a Bruker D8 DISCOVER diffractometer (Bruker, Billerica, MA, USA), Cu-Kα = 1.5406 Å. Grazing incidence XRD (GIXRD) modes, that are surface sensitive, were used for XRD measurements using a 2θ range of 20–65° in 0.1° steps and 1 s exposure at each step. The angle of incidence of the primary X-ray beam was 0.7°. XRR measurements were carried out over an angular range of 0.2–5° (0.01° step) using symmetric scattering geometry. The results were processed by the Rietveld method using the TOPAS software package (version 5, Bruker, Billerica, MA, USA) and LEPTOS (version 7.7, Bruker, Billerica, MA, USA) for XRD and XRR, respectively. The approximate thickness, density, and the number of coatings and instrumental parameters (radiation wavelength, goniometer radius, slit width, etc.) were set using the LEPTOS software. Based on these data, the theoretical curve was modeled and fitted to best match with experimental data using the simplex method by varying the characteristics of the samples (roughness, thickness, and density). The χ^2 value for the modeled curve was 8.080×10^{-3}.

X-ray photoelectron spectra (XPS) were obtained on an Escalab 250Xi spectrometer (Thermo Fisher Scientific, Waltham, MA, USA). To obtain information about inner layers of the deposited film the Ar+ sputtering (500 eV for 90 s) was performed. The samples were excited by the X-ray radiation Al-Kα (1486.7 eV) at a pressure of 7×10^{-8} Pa.

The scanning electron micrographs of flat and cross-sections were obtained by a Supra 55 VP scanning electron microscope (SEM, Zeiss, Oberkochen, Germany) with a Gemini-I column and a field emission cathode. The spatial resolution was about 1.3 nm at an accelerating voltage of 3 kV. A total of 3 randomly selected positions on the sample surface were examined. An Everhart-Thornley and an InLens secondary electron detectors were used for SEM studies. Energy Dispersive X-ray (EDX) analysis was performed using an INCA X-Max system (Oxford Instruments, High Wycombe, UK) mounted on a Supra 55 VP SEM.

Stainless steel plates (SS) with deposited films were used for electrochemical studies. Lithium foil, polyolefin porous film 2325 (Celgard, Charlotte, NC, USA), and TC-E918 (Tinci, Guangzhou, China) were used as a counter electrode, a separator and an electrolyte, respectively. The composition TC-E918 was a 1M solution of $LiPF_6$ in a mixture of organic carbonates (ethylene carbonate, propylene carbonate, diethyl carbonate, ethyl methyl carbonate, vinyl carbonate). The coin cells (CR2032) were assembled in OMNI-LAB (VAC) glove box under argon atmosphere. Cyclic voltammetry (CV) was performed using a PGSTAT302N + potentiostat (Autolab, Utrecht, The Netherlands) in the range 0.01–4.30 V with a scan rate of 0.5 mV/s.

3. Results and Discussions

3.1. Atomic Layer Deposition of Ta-O Thin Films

To determine the optimal conditions for the tantalum oxide growth, the effect of the $Ta(OEt)_5$ evaporator temperature, the time of pulsing, purging and the reactor temperature on the GPC were studied (Table 2).

Table 2. Conditions of the ALD process for obtaining the Ta-O system.

No	Reagent Temperature °C	Time Pulse/Purge, s	Reactor Temperature °C	Number of Cycles	GPC nm/cycle
Ta-O_1	70	1/5	300	500	0.0041
Ta-O_2	90	1/5	300	500	0.0057
Ta-O_3	110	1/5	300	500	0.0093
Ta-O_4	160	1/5	300	500	0.0433
Ta-O_5	190	1/5	300	500	0.0486
Ta-O_6	190	1.5/5	300	1000	0.0463
Ta-O_7	190	0.5/5	300	500	0.0426
Ta-O_8	190	2/5	300	500	0.0464
Ta-O_9	190	1/10	300	500	0.0439
Ta-O_10	190	1/15	300	500	0.0472
Ta-O_11	190	1.5/10	300	500	0.0501
Ta-O_12	190	1/5	225	500	0.0547
Ta-O_13	190	1/5	250	500	0.0502
Ta-O_14	190	1/5	350	500	0.0467
Ta-O_15	190	1/5	300	50	0.0780
Ta-O_16	190	1/5	300	100	0.0600
Ta-O_17	190	1/5	300	200	0.0505

There was a low growth per cycle (less than 0.01 nm/cycle) at the evaporator temperatures from 70 °C to 110 °C, indicating that the evaporator temperature is insufficient for the required amount of the reagent enters the reactor (Figure 1a). At 160 °C and 190 °C, the average growth per cycle increases up to 0.043–0.049 nm/cycle and begin to stabilize. The further increasing temperature is not technically possible because of equipment limitations. Thus, it is necessary to heat the evaporator to at least 190 °C to carry out the tantalum oxide synthesis.

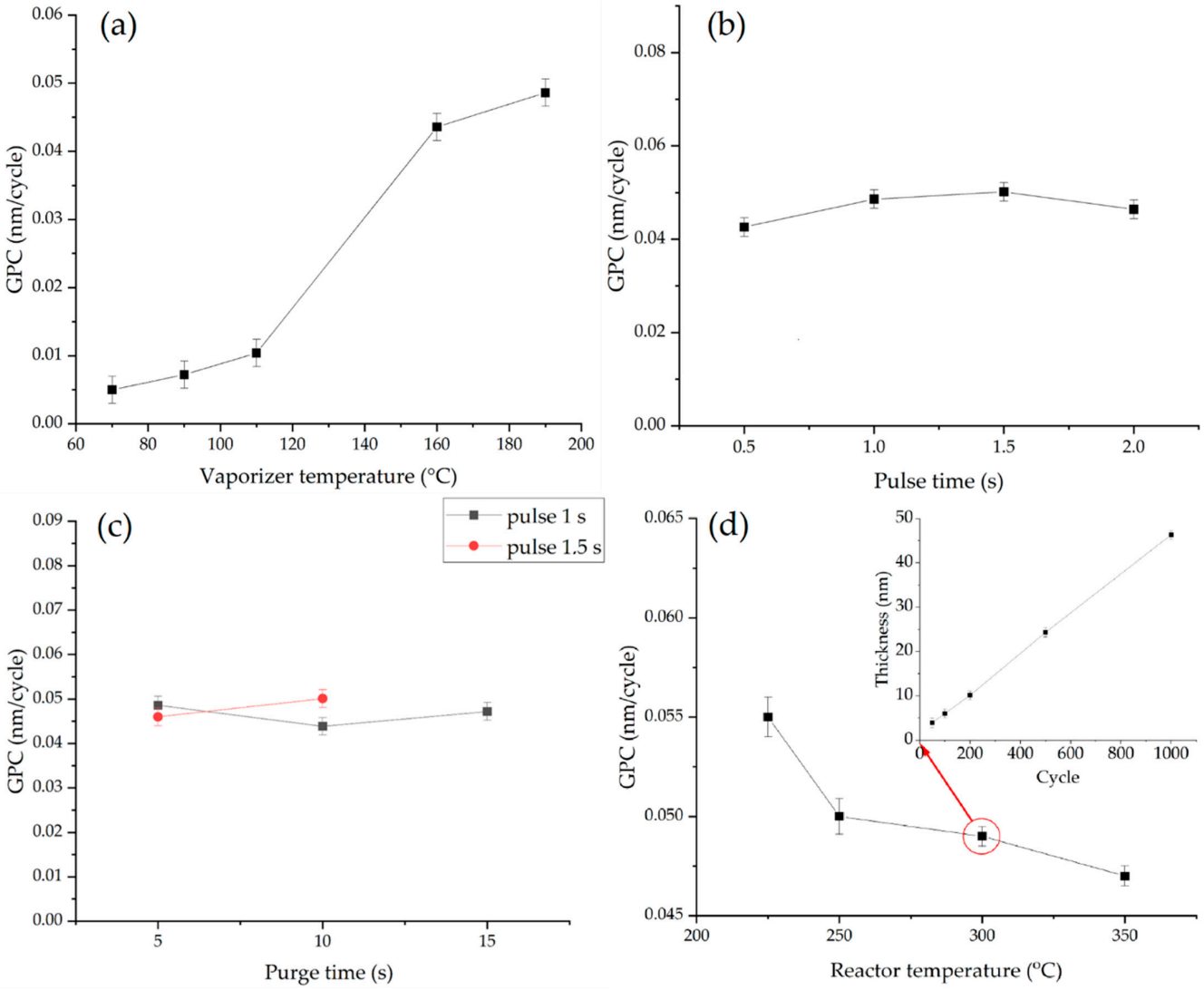

Figure 1. (**a**) The effect of vaporizer temperature (pulse 1 s, purge 5 s, reactor 300 °C) on the GPC; (**b**) The GPC as a function of pulse time (purge 5 s, evaporator 190 °C; reactor 300 °C); (**c**) The influence of reactor purge time for pulses of 1 and 1.5 s (evaporator 190 °C, reactor 300 °C) on GPC; (**d**) The GPC depending from reactor temperature (pulse 1 s, purge 5 s). Inset shows the change in Ta-O film thickness versus number of cycles (pulse 1 s, purge 5 s, evaporator and reactor temperature were 190 °C and 300 °C, correspondingly).

The dependences of the average growth per cycle from the $Ta(OEt)_5$ pulse time were studied to determine the reactor filling time required to reach saturation. The experiments were carried out at a constant reactor temperature (300 °C) and purging times (after $Ta(OEt)_5$ pulse in 5 s, after plasma treatment in 15 s). With an increase of the $Ta(OEt)_5$ pulse duration from 0.5 to 1.0 s, the value of the average growth per cycle augments from 0.042 to 0.049 nm/cycle, and after subsequent pulse time increase GPC does not grow (Figure 1b). Further increases pulse up to 2 s resulted in a slight decrease in the average growth per cycle. Thus, the saturation of the substrate precursor vapors under synthesis conditions can be achieved with a $Ta(OEt)_5$ pulse time of more than 1.0 s.

To determine the effect of purge duration two series of samples were prepared with 1.0 s and 1.5 s of reactor filling time of $Ta(OEt)_5$ were chosen (Figure 1c). The purge duration for both series of samples was set to 5 s, 10 s, 15 s. For both series of samples, the average growth rate was almost the same. Thus, neither adsorption time nor desorption time doesn't influence on the growth rate. We can assume that all available functional groups

react during adsorption carried out during 1 s. And 5 s is sufficient to eliminate all excess of $Ta(OEt)_5$ adsorbed during less or equal 1.5 s.

The average growth per cycle dependences on the reactor temperature were studied to determine the temperature window of the synthesis (Figure 1d). With an increase of the reactor temperature from 225 °C to 350 °C, the average growth per cycle value decreases from 0.055 to 0.047 nm/cycle. It was determined that the largest growth per cycle was at 225 °C (0.055 nm/cycle). The high average growth per cycle value is probably a consequence of the precursor condensation on the substrate surface due to the relatively low reactor temperature and the small difference between the temperatures in the $Ta(OEt)_5$ evaporator and the reactor. The average growth per cycle values decreases to 0.049–0.050 nm/cycle in the 250 °C. After which in the temperature range of 250–300 °C remains close to constant. The growth per cycle decreases with an increase in temperature, which may be caused by a decrease in the number of functional groups.

The interval in the temperature range 250–300 °C can be considered as a "synthesis window" for ALD processes using $Ta(OEt)_5$ and oxygen plasma because of the constant growth rate (0.049–0.050 nm/cycle). The linear dependence of the tantalum oxide layer thickness on the number of ALD cycles indicates the absence of nucleation growth effects and the possibility of the film thickness precise control (Figure 1d inset). The obtained growth per cycle values are less than GPC showed in [8] (0.075 nm/cycle), where $Ta(OEt)_5$ and oxygen plasma were used as reagents. However, they are very close to the growth per cycle values (0.049 nm/cycle) obtained with water as a co-reagent at a temperature of 300 °C (Table 1). The slight difference between the experimental and published data is probably due to the design differences of the used setups, the thickness measurement techniques.

3.2. Morphology of Films on Si

Top view and cross-sectional images of Ta-O films on a Si substrate, obtained using scanning electron microscopy, are shown in Figure 2. The resulting tantalum oxide films were smooth and homogeneous, without visible defects and inclusions. The average thickness sample of Ta O_6 is about 46.3 nm. The smoothness of the film indicates the absence of nucleation effects during synthesis in the ALD "window".

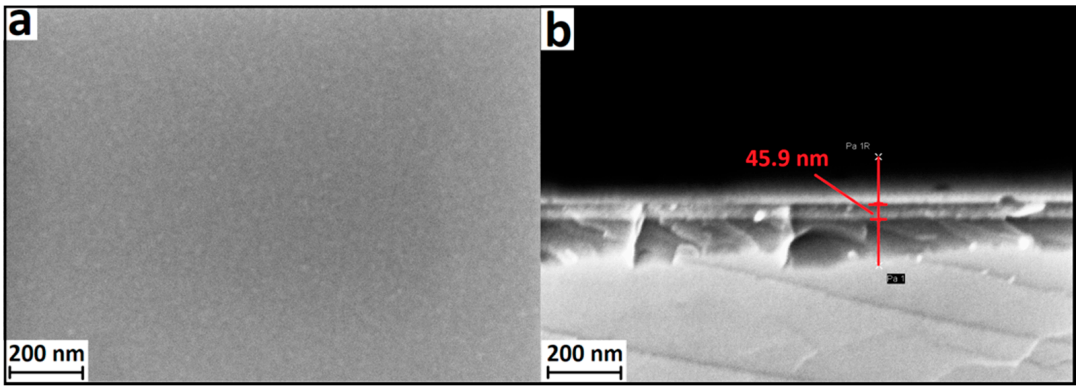

Figure 2. SEM of the surface (**a**) and cleavage (**b**) of the Ta-O_6 sample on a Si substrate.

3.3. Chemical Composition of the Films

The EDX analysis was carried out to determine the chemical composition. It showed that the atomic concentration ratio of Ta:O in the film (with a thickness of 46.3 nm) is approximately 1:2.7. The observed ratio indicates the formation of tantalum (V) oxide during the synthesis. It can be concluded that there is no reduction of tantalum during the synthesis since $Ta(OEt)_5$ was used for the deposition. The slight excess of the oxygen atomic concentration over ratios 2:5 may be due to a natural oxide layer on the silicon substrate surface.

A decrease in the energy of exciting radiation during the EDX makes it possible to reduce the depth of the analyzed region. Considering the small thickness of the analyzed coatings (3.9–46.3 nm), the minimum accelerating voltage of 3 kV was chosen to study the samples.

A clear signal from tantalum is observed even on the X-ray spectra with a coating thickness of 6 nm (Figure 3). As the film thickness increases, the main peak of tantalum (M-series) shifts to the low-energy side due to the decrease in the effect of the silicon substrate. The intensity of the peaks in the spectral regions of 1.335 and 1.96 keV also increases. The intensity of the maxima corresponding to silicon atoms decreases.

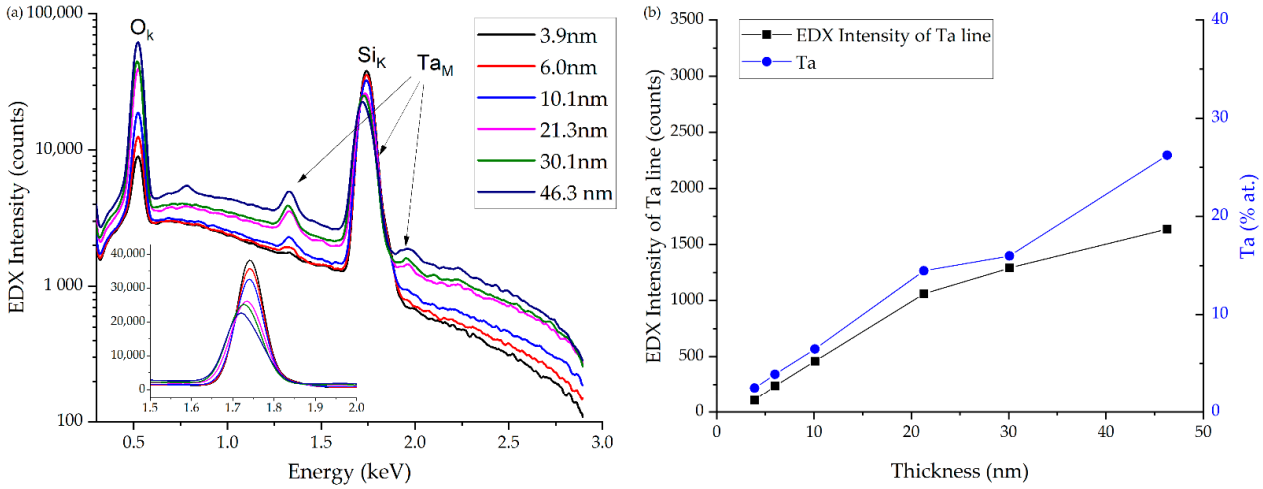

Figure 3. (**a**) EDX spectra of tantalum oxide samples of various thicknesses deposited on silicon with linear and logarithmic dependences. (**b**) Dependence of the 1.335 keV tantalum line intensity and atomic content on the film thickness.

A sample of tantalum oxide (Ta-O_11), obtained at the reactor temperature of 300 °C during 500 cycles, was investigated by the XPS method for a detailed study of the chemical composition. Both the external surface and the coating volume were studied after etching the surface layer with argon ions. Tantalum, oxygen, and carbon were found on the sample surface (Table 3). After the surface layer etching, carbon peaks in the spectrum are no longer observed, indicating that there is no carbon in the coating. Presumably, the sample surface is contaminated with organic and inorganic carbon compounds deposited from the air.

Table 3. Atomic ratios of elements before and after etching according to XPS data.

Spectra	Before Etching, at. %	After Etching, at. %
O1s	52.46	48.89
Ta4f	20.64	51.11
C1s	26.90	0

Based on the C1s level peak position and shape, carbon on the sample surface is predominantly in the C–C, C–H state (Figure 4). In addition, there is a small amount of C–OH. There are no compounds with C=O bonds, COOH, and carbonates on the surface. The O1s spectra of the surface exhibit an intense peak corresponding to Ta_2O_5 and a small shoulder corresponding to compounds with C–O bonds. This peak shifts toward the higher energies during etching. According to the fact that no carbon was found in the etched sample and it cannot contain oxygen-containing phases C–O and C=O, the shift is caused by the reduction of Ta_2O_5 to intermediate oxide phases TaO, Ta_2O_3.

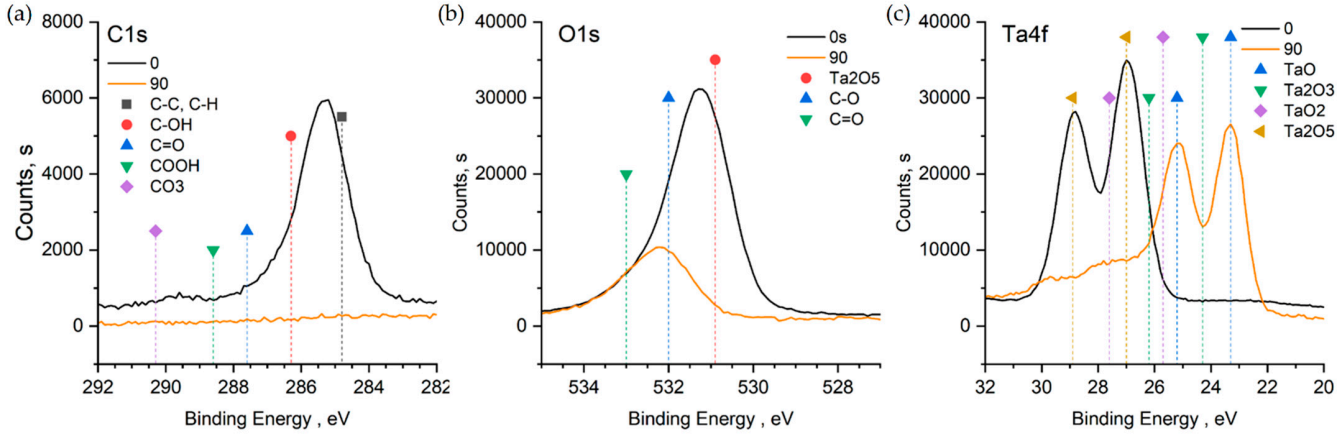

Figure 4. XPS spectrum for Ta-O_11 C1s (**a**), O1s (**b**), Ta4f (**c**).

According to the XPS spectra of the Ta4f level, Ta_2O_5 is located on the sample surface. The Ta to O 2:5 ratio also corresponds to this compound and coincides with the data obtained by the EDX. The peaks shift to the lower energies after etching, their maxima correspond to the TaO compound, and the Ta to O ratio becomes 1:1. According to the XRD data, the film volume consists of Ta_2O_5. Judging by that, it is likely that TaO was a result of the Ta^{5+} reduction upon bombardment with the argon ions.

3.4. Crystal Structure

The XRD of the sample showed that the resulting films in ALD "window" are amorphous, Figure 5. In the range from 20 to 40° 2θ, a diffuse halo is noticeable. It signifies the crystallization onset of the tantalum (V) oxide phase. The fact that there are no metallic tantalum peaks indicates its absence in the film composition. It correlates with the data obtained by the XPS, in the spectra, the maxima corresponding to tantalum in the zero-oxidation state were not found. After heat treatment (HT) at 800 °C for 15 min, intense peaks appeared in the diffractogram at 23, 29, 37.5, 45, 47, 51, and 56°, corresponding to the crystalline phase of Ta_2O_5 (orthorhombic, Pmm2). According to the ellipsometry data, the films' thickness before and after HT is not changed within the measurement accuracy (Supplementary file, Figure S3) thus we can assume that remains stable and cover substrate even after calcination at high temperature.

The X-ray reflectometry of the sample before HT (Figure 6) showed that the films have a uniform density equal to 7.98 g/cm^3, close to 7.96 g/cm^3 [42], and close to the crystal Ta_2O_5 density of 8.18 g/cm^3 [43]. The lower density is due to the amorphous state of the tantalum (V) oxide. According to the XRR data, the films have low roughness, which is also confirmed by the SEM photography. The film thickness was 46.8 nm, close to the data obtained by spectral ellipsometry (46.3 nm).

3.5. SEM of Tantalum Oxide Coated Steel

The surface of coatings deposited on the steel substrates differs from the sample deposited on silicon. The densely spaced particles ranging in size from several tens to one hundred nanometers (Figure 7) are presented on the surface. The average thickness of Ta-O_6 coating on the stainless steel is about 61.4 nm. The difference in the morphology of coatings on silicon and steel may be due to different surface roughness and functional groups of a different nature. The average growth per cycle is 0.0614 nm/cycle, that more GPC on the silicon surface (0.0463 nm/cycle).

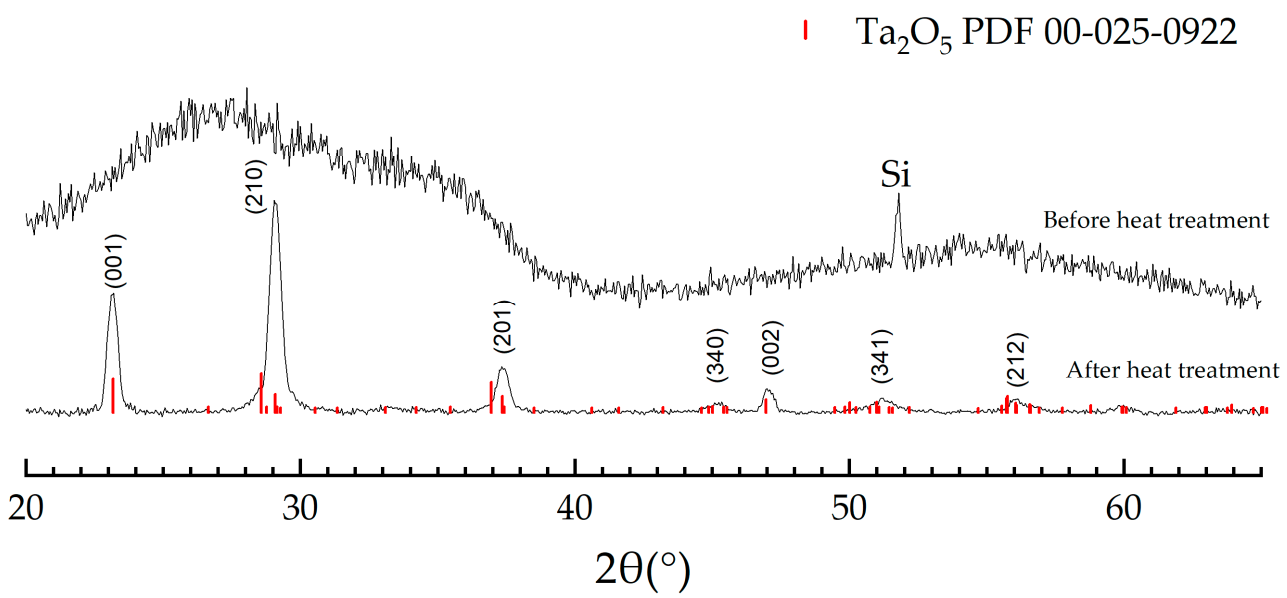

Figure 5. XRD of Ta-O films before and after HT.

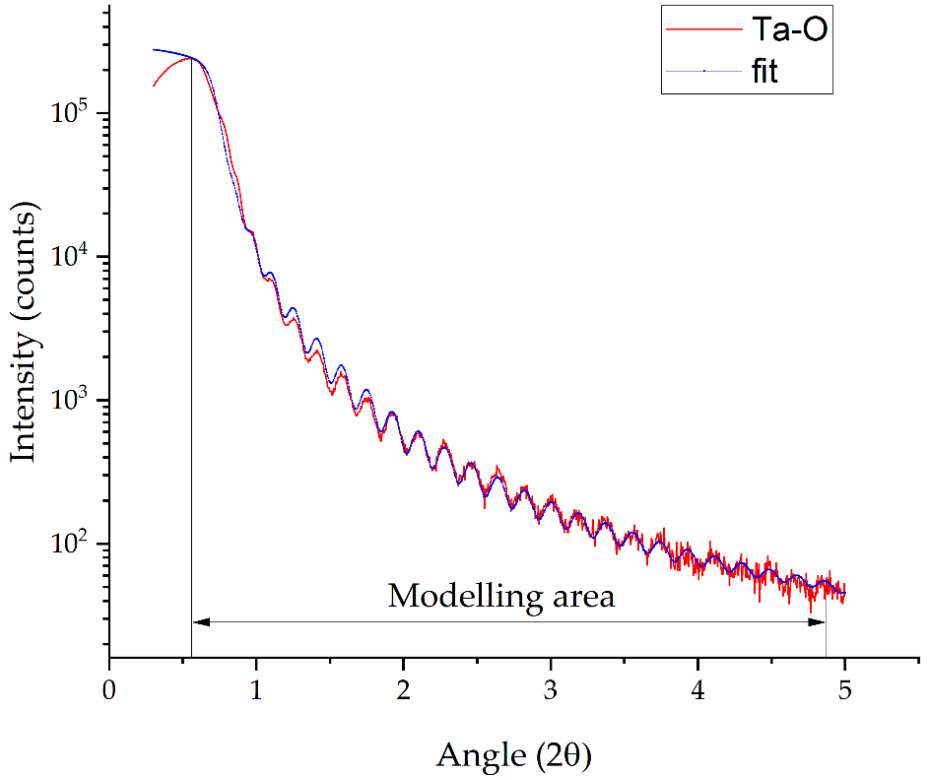

Figure 6. X-ray reflectometry of the Ta-O_6 sample before HT.

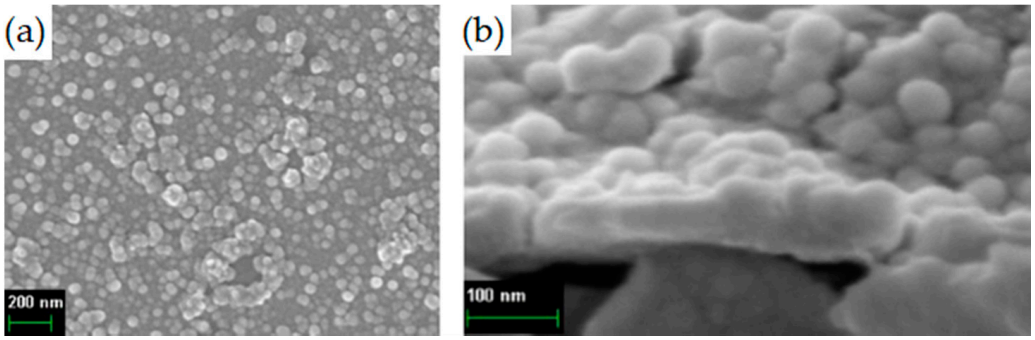

Figure 7. SEM of the surface (**a**) and cleavage (**b**) of the Ta-O_6 sample on a steel substrate.

3.6. Electrochemical Studies

Cyclic voltammetry (CV) was carried out for samples of amorphous tantalum (V) oxide on steel substrates (TaO_9). The results of 5 cycles of CV are shown in Figure 8.

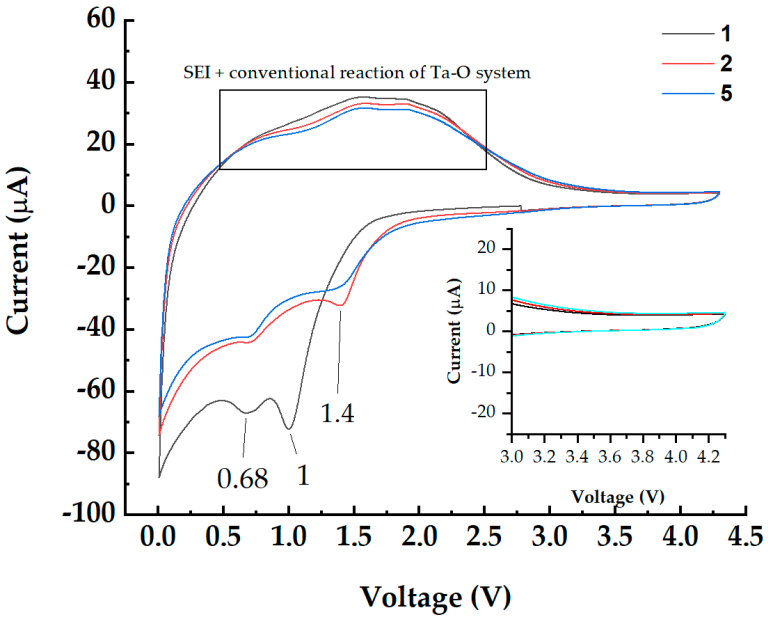

Figure 8. CV of coatings of the Ta-O system in the potential window of 4.3–0.1 V.

During CV scans of nanofilms, a pronounced current increase appeared in the 3.0–0.1 V range. It was caused by conventional reactions and lithiation of Ta-O nanofilms [44], and a partial reduction in organic solvents (ethylene carbonate, propylene carbonate, diethyl carbonate, ethyl methyl carbonate) and functional additives (vinylene carbonate) of electrolytes with the formation of a gel-like solid electrolyte interface (SEI) film on the active layer [45]. However, there is no current amplification in the cathode potential range (4.3–3.0 V) (inset in Figure 8). Thus, the investigated coatings do not affect the electrochemical capacity in the region of cathodic potentials and do not interact with the electrolyte. In the works, the stabilization of Ni-rich cathodes is shown both when doping with tantalum [46] and when applying tantalum-containing oxide coatings [47]. Thus, they can be used as protective coatings for cathode materials [2].

4. Conclusions

As a result, the optimal conditions for the production of tantalum (V) oxide nanofilms by the ALD were determined. The temperature effect of the container's evaporator with the reagent $Ta(OEt)_5$, the time of its pulsing, purging, and the reactor temperature on the growth per cycle were studied. The results showed that to achieve the ALD growth of the substrate surface with $Ta(OEt)_5$ vapors, an evaporator temperature above 190 °C and an

pulse time of at least 1 s are required. A 5 s purge is sufficient to remove excess reagent and reaction products. The ALD temperature window is 250–300 °C, with an average growth per cycle at 0.043–0.050 nm/cycle.

The study of the obtained nanofilms by XPS and EDX showed that the films contain no unreacted carbon-containing residues of the $Ta(OEt)_5$ precursor, and the stoichiometric ratio of tantalum and oxygen is close to Ta_2O_5. The nanofilms deposited on Si substrates have homogeneous morphology, low roughness, and the density (7.98 g/cm^3) are close to bulk tantalum (V) oxide (8.18 g/cm^3). The nanofilms obtained at 300 °C with a thickness of 46–47 nm are X-ray amorphous. However, they crystallize upon annealing at 800 °C with the formation of orthorhombic Ta_2O_5.

The average growth per cycle of nanofilms on stainless steel is 0.0614 nm/cycle, which is more than GPC on the silicon surface (0.0463 nm/cycle). This nanofilms are not homogenous and consist of densely spaced particles ranging from several tens to one hundred nanometers.

The obtained cyclic voltammograms analysis of the nanofilms deposited on steel substrates showed that the coatings in the cathode potential range (4.3–3.0 V) do not interact with the electrolyte and do not contribute to the electrochemical capacity.

Supplementary Materials: The following are available online at https://www.mdpi.com/article/10.3390/coatings11101206/s1, Figure S1: The measured and calculated spectra of ellipsometric angles ψ (a) and Δ (b) at an angle of incidence φ = 70° for a Ta-O layer with a thickness of d = 46.3 nm, Figure S2: According to the ellipsometric angles, the real ε1 and imaginary ε2 parts of the complex dielectric function for the ALD Ta-O sample with the layer thickness d = 46 nm were calculated by Cauchy model. Comparison with the data from for Ta-O deposited layer (d = 48 nm) by evaporation of tantalum in atomic oxygen plasma. In both cases, there was a Si substrate, Figure S3. Ellipsometric angles ψ (a) and Δ (b) for the TaO sample before and after annealing (800 °C) and the corresponding dependences of the real part of the dielectric function ε1 (c).

Author Contributions: Conceptualization, M.Y.M., Y.K.; methodology, M.Y.M.; supervision, M.Y.M.; project administration, M.Y.M.; validation, M.Y.M., Y.K.; data curation, M.Y.M., formal analysis, D.N.; investigation, P.F., D.N., V.T., A.R.; writing—review & editing, M.Y.M., Y.K., P.F., D.N.; writing—original draft, P.F., D.N., V.T., O.M.; visualization, P.F., V.T., O.M.; formal analysis, V.T., O.M., A.R.; re-sources, M.Y.M., A.P.; funding acquisition, M.Y.M. All authors have read and agreed to the published version of the manuscript.

Funding: The research is partially funded by the Ministry of Science and Higher Education of the Russian Federation: Advanced Digital Technologies (contract No. 075-15-2020-934 dated 17 November 2020).

Data Availability Statement: Data available on request due to restrictions on privacy. The data presented in this study are available on request from the corresponding author.

Acknowledgments: This research was conducted using the equipment of the resource centers of the Research Park of the St. Petersburg State University, "Innovative Technologies of Composite Nanomaterials", "Physical Methods of Surface Investigation", "X-ray Diffraction Studies", and "Nanotechnology".

Conflicts of Interest: The authors declare no conflict of interest.

References

1. Pfeiffer, K.; Schulz, U.; Tünnermann, A.; Szeghalmi, A. Antireflection coatings for strongly curved glass lenses by atomic layer deposition. *Coatings* **2017**, *7*, 118. [CrossRef]
2. Rossnagel, S.M.; Sherman, A.; Turner, F. Plasma-enhanced atomic layer deposition of Ta and Ti for interconnect diffusion barriers. *J. Vac. Sci. Technol. B Microelectron. Nanom. Struct.* **2000**, *18*, 2016. [CrossRef]
3. Malygin, A.A.; Drozd, V.E.; Malkov, A.A.; Smirnov, V.M. From V. B. Aleskovskii's "framework" Hypothesis to the Method of Molecular Layering/Atomic Layer Deposition. *Chem. Vap. Depos.* **2015**, *21*, 216–240. [CrossRef]
4. Maximov, M.; Nazarov, D.; Rumyantsev, A.; Koshtyal, Y.; Ezhov, I.; Mitrofanov, I.; Kim, A.; Medvedev, O.; Popovich, A. Atomic layer *Depos.* of lithium-nickel-silicon oxide cathode material for thin-film lithium-ion batteries. *Energies* **2020**, *13*, 2345. [CrossRef]

5. Metalorganics.Ru. Available online: http://www.metalorganics.ru/files/PR-ME-R/PR-TA1-R2.htm (accessed on 13 August 2021).
6. Kukli, K.; Ritala, M.; Leskelä, M. Atomic layer deposition and chemical vapor deposition of tantalum oxide by successive and simultaneous pulsing of tantalum ethoxide and tantalum chloride. *Chem. Mater.* **2000**, *12*, 1914–1920. [CrossRef]
7. Kariniemi, M.; Niinistö, J.; Vehkamäki, M.; Kemell, M.; Ritala, M.; Leskelä, M.; Putkonen, M. Conformality of remote plasma-enhanced atomic layer deposition processes: An experimental study. *J. Vac. Sci. Technol. A Vacuum Surf. Film.* **2012**, *30*, 01A115. [CrossRef]
8. Song, H.J.; Lee, C.S.; Kang, S.W. Increment of the dielectric constant of Ta_2O_5 thin films by retarding interface oxide growth on Si substrates. *Electrochem. Solid-State Lett.* **2001**, *4*, 13–14. [CrossRef]
9. Sønsteby, H.H.; Nilsen, O.; Fjellvåg, H. Atomic layer deposition of (K,Na) (Nb,Ta)O_3 thin films. *J. Vac. Sci. Technol. A Vacuum Surf. Film* **2016**, *34*, 041508. [CrossRef]
10. Liu, J.; Banis, M.N.; Li, X.; Lushington, A.; Cai, M.; Li, R.; Sham, T.K.; Sun, X. Atomic layer deposition of lithium tantalate solid-state electrolytes. *J. Phys. Chem. C* **2013**, *117*, 20260–20267. [CrossRef]
11. Gu, D.; Li, J.; Dey, S.K.; De Waard, H.; Marcus, S. Nanochemistry, nanostructure, and electrical properties of Ta_2O_5 film deposited by atomic layer deposition and plasma-enhanced atomic layer deposition. *J. Vac. Sci. Technol. B Microelectron. Nanom. Struct.* **2006**, *24*, 2230. [CrossRef]
12. Alimardani, N.; King, S.W.; French, B.L.; Tan, C.; Lampert, B.P.; Conley, J.F. Investigation of the impact of insulator material on the performance of dissimilar electrode metal-insulator-metal diodes. *J. Appl. Phys.* **2014**, *116*, 024508. [CrossRef]
13. Egorov, K.V.; Kuzmichev, D.S.; Chizhov, P.S.; Lebedinskii, Y.Y.; Hwang, C.S.; Markeev, A.M. In Situ Control of Oxygen Vacancies in TaOx Thin Films via Plasma-Enhanced Atomic Layer Deposition for Resistive Switching Memory Applications. *ACS Appl. Mater. Interfaces* **2017**, *9*, 13286–13292. [CrossRef] [PubMed]
14. Egorov, K.V.; Kuzmichev, D.S.; Sigarev, A.A.; Myakota, D.I.; Zarubin, S.S.; Chizov, P.S.; Perevalov, T.V.; Gritsenko, V.A.; Hwang, C.S.; Markeev, A.M. Hydrogen radical enhanced atomic layer deposition of TaO_x: Saturation studies and methods for oxygen deficiency control. *J. Mater. Chem. C* **2018**, *6*, 9667–9674. [CrossRef]
15. Yang, W.S.; Kang, S.W. Comparative study on chemical stability of dielectric oxide films under HF wet and vapor etching for radiofrequency microelectromechanical system application. *Thin Solid Films* **2006**, *500*, 231–236. [CrossRef]
16. Kukli, K.; Kemell, M.; Vehkamäki, M.; Heikkilä, M.J.; Mizohata, K.; Kalam, K.; Ritala, M.; Leskelä, M.; Kundrata, I.; Fröhlich, K. Atomic layer deposition and properties of mixed Ta_2O_5 and ZrO_2 films. *AIP Adv.* **2017**, *7*, 025001. [CrossRef]
17. Kim, M.K.; Kim, W.H.; Lee, T.; Kim, H. Growth characteristics and electrical properties of Ta_2O_5 grown by thermal and O_3-based atomic layer deposition on TiN substrates for metal-insulator-metal capacitor applications. *Thin Solid Films* **2013**, *542*, 71–75. [CrossRef]
18. Jenkins, M.A.; Austin, D.Z.; Holden, K.E.K.; Allman, D.; Conley, J.F. Laminate Al_2O_3/Ta_2O_5 Metal/Insulator/Insulator/Metal (MIIM) Devices for High-Voltage Applications. *IEEE Trans. Electron Devices* **2019**, *66*, 5260–5265. [CrossRef]
19. Ma, P.; Lu, J.; Aubuchon, J.; Gung, T.-J.; Chang, M. (Invited) Plasma Enhanced Atomic Layer Deposition of TaN Films for Advanced Interconnects. *ECS Trans.* **2019**, *33*, 169–176. [CrossRef]
20. Kwon, J.D.; Park, J.S.; Lee, H.C.; Kang, S.W. A chemical reaction path design for the atomic layer deposition of tantalum nitride thin films. *Electrochem. Solid-State Lett.* **2006**, *9*, 282–284. [CrossRef]
21. Chung, H.-S.; Kwon, J.-D.; Kang, S.-W. Plasma-Enhanced Atomic Layer Deposition of TaN Thin Films Using Tantalum-Pentafluoride and N_2H_2Ar Plasma. *J. Electrochem. Soc.* **2006**, *153*, C751. [CrossRef]
22. Chaker, A.; Vallee, C.; Pesce, V.; Belahcen, S.; Vallat, R.; Gassilloud, R.; Posseme, N.; Bonvalot, M.; Bsiesy, A. Topographically selective deposition. *Appl. Phys. Lett.* **2019**, *114*, 043101. [CrossRef]
23. Choi, B.J.; Zhang, J.; Norris, K.; Gibson, G.; Kim, K.M.; Jackson, W.; Zhang, M.X.M.; Li, Z.; Yang, J.J.; Williams, R.S. Trilayer Tunnel Selectors for Memristor Memory Cells. *Adv. Mater.* **2016**, *28*, 356–362. [CrossRef]
24. Fang, Q.; Hodson, C.; Liu, M.; Fang, Z.W.; Potter, R.; Gunn, R. Preliminary Investigation of High-K Materials-TiO_2 Doped Ta_2O_5 Films by Remote Plasma Ald. *Phys. Procedia* **2012**, *32*, 379–388. [CrossRef]
25. Song, S.J.; Park, T.; Yoon, K.J.; Yoon, J.H.; Kwon, D.E.; Noh, W.; Lansalot-Matras, C.; Gatineau, S.; Lee, H.K.; Gautam, S.; et al. Comparison of the atomic layer deposition of tantalum oxide thin films using Ta(NtBu)$(NEt_2)_3$, Ta(NtBu)$(NEt_2)_2$Cp, and H_2O. *ACS Appl. Mater. Interfaces* **2017**, *9*, 537–547. [CrossRef] [PubMed]
26. Kim, S.-W.; Kwon, S.-H.; Jeong, S.-J.; Kang, S.-W. Improvement of Copper Diffusion Barrier Properties of Tantalum Nitride Films by Incorporating Ruthenium Using PEALD. *J. Electrochem. Soc.* **2008**, *155*, H885. [CrossRef]
27. Park, T.J.; Kim, J.H.; Jang, J.H.; Na, K.D.; Hwang, C.S.; Kim, G.M.; Choi, K.J.; Jeong, J.H. Effective work function tunability and interfacial reactions with underlying HfO_2 layer of plasma-enhanced atomic layer deposited TaC_xN_y films. *Appl. Phys. Lett.* **2008**, *92*, 12–15. [CrossRef]
28. Park, T.J.; Kim, J.H.; Jang, J.H.; Na, K.D.; Hwang, C.S.; Kim, J.H.; Kim, G.M.; Choi, J.H.; Choi, K.J.; Jeong, J.H. Improved electrical performances of plasma-enhanced atomic layer deposited TaCx Ny films by adopting Ar H_2 plasma. *Appl. Phys. Lett.* **2007**, *91*, 2005–2008. [CrossRef]
29. Lee, H.J.; Park, J.S.; Kwon, S.H. Plasma-enhanced atomic layer deposition of tantalum nitride thin films using tertiary-amylimido-tris(dimethylamido)tantalum and hydrogen plasma. *J. Electroceram.* **2016**, *36*, 165–169. [CrossRef]

30. Nabatame, T.; Ohi, A.; Ito, K.; Takahashi, M.; Chikyo, T. Role of the (Ta/Nb)Ox/Al_2O_3 interface on the flatband voltage shift for Al_2O_3/(Ta/Nb)Ox/Al_2O_3 multilayer charge trap capacitors. *J. Vac. Sci. Technol. A Vacuum Surf. Film* **2015**, *33*, 01A118. [CrossRef]
31. Heil, S.B.S.; Roozeboom, F.; van de Sanden, M.C.M.; Kessels, W.M.M. Plasma-assisted atomic layer deposition of Ta_2O_5 from alkylamide precursor and remote O_2 plasma. *J. Vac. Sci. Technol. A Vac. Surf. Film* **2008**, *26*, 472–480. [CrossRef]
32. Yoon, J.H.; Kim, K.M.; Song, S.J.; Seok, J.Y.; Yoon, K.J.; Kwon, D.E.; Park, T.H.; Kwon, Y.J.; Shao, X.; Hwang, C.S. Pt/Ta_2O_5/HfO_2-x/Ti Resistive Switching Memory Competing with Multilevel NAND Flash. *Adv. Mater.* **2015**, *27*, 3811–3816. [CrossRef]
33. Han, J.H.; Kim, H.Y.; Lee, S.C.; Kim, D.H.; Park, B.K.; Park, J.S.; Jeon, D.J.; Chung, T.M.; Kim, C.G. Growth of tantalum nitride film as a Cu diffusion barrier by plasma-enhanced atomic layer deposition from bis((2-(dimethylamino)ethyl)(methyl)amido)methyl(tert-butylimido)tantalum complex. *Appl. Surf. Sci.* **2016**, *362*, 176–181. [CrossRef]
34. Kim, H.; Lavoie, C.; Copel, M.; Narayanan, V.; Park, D.G.; Rossnagel, S.M. The physical properties of cubic plasma-enhanced atomic layer deposition TaN films. *J. Appl. Phys.* **2004**, *95*, 5848–5855. [CrossRef]
35. Kim, H.; Cabral, C.; Lavoie, C.; Rossnagel, S.M. The Growth of Tantalum Thin Films by Plasma-Enhanced. *Mater. Res.* **2002**, *716*, B8.5.
36. Kim, H.; Kellock, A.J.; Rossnagel, S.M. Growth of cubic-TaN thin films by plasma-enhanced atomic layer deposition. *J. Appl. Phys.* **2002**, *92*, 7080–7085. [CrossRef]
37. Chang, C.-C.; Pan, F.-M.; Chen, C.-W. Effect of Surface Reduction Treatments of Plasma-Enhanced Atomic Layer Chemical Vapor Deposited TaN_x on Adhesion with Copper. *J. Electrochem. Soc.* **2010**, *157*, G62. [CrossRef]
38. Kim, H.; Rossnagel, S.M. Plasma-enhanced atomic layer deposition of tantalum thin films: The growth and film properties. *Thin Solid Films* **2003**, *441*, 311–316. [CrossRef]
39. Kim, H.; Cabral, C.; Lavoie, C.; Rossnagel, S.M. Diffusion barrier properties of transition metal thin films grown by plasma-enhanced atomic-layer deposition. *J. Vac. Sci. Technol. B Microelectron. Nanom. Struct.* **2002**, *20*, 1321. [CrossRef]
40. Fujiwara, H. *Spectroscopic Ellipsometry: Principles and Applications*; John Wiley & Sons: Hoboken, NJ, USA, 2007; pp. 1–369. [CrossRef]
41. Järrendahl, K.; Arwin, H. Multiple sample analysis of spectroscopic ellipsometry data of semi-transparent films. *Thin Solid Films* **1998**, *313–314*, 114–118. [CrossRef]
42. Damart, T.; Coillet, E.; Tanguy, A.; Rodney, D. Numerical study of the structural and vibrational properties of amorphous Ta_2O_5 and TiO_2-doped Ta_2O_5. *J. Appl. Phys.* **2016**, *119*, 175106. [CrossRef]
43. Reisman, A.; Holtzberg, F.; Berkenblit, M.; Berry, M. Reactions of the Group VB Pentoxides with Alkali Oxides and Carbonates. III. Thermal and X-Ray Phase Diagrams of the System K_2O or K_2CO_3 with Ta_2O_5. *J. Am. Chem. Soc.* **1956**, *78*, 4514–4520. [CrossRef]
44. Manukumar, K.N.; Kishore, B.; Manjunath, K.; Nagaraju, G. Mesoporous Ta_2O_5 nanoparticles as an anode material for lithium ion battery and an efficient photocatalyst for hydrogen evolution. *Int. J. Hydrogen Energy* **2018**, *43*, 18125–18135. [CrossRef]
45. Koshtyal, Y.; Nazarov, D.; Ezhov, I.; Mitrofanov, I.; Kim, A.; Rymyantsev, A.; Lyutakov, O.; Popovich, A.; Maximov, M. Atomic layer deposition of nio to produce active material for thin-film lithium-ion batteries. *Coatings* **2019**, *9*, 301. [CrossRef]
46. Jamil, S.; Yu, R.; Wang, Q.; Fasehullah, M.; Huang, Y.; Yang, Z.; Yang, X.; Wang, X. Enhanced cycling stability of nickel-rich layered oxide by tantalum doping. *J. Power Sources* **2020**, *473*, 228597. [CrossRef]
47. Li, X.; Liu, J.; Banis, M.N.; Lushington, A.; Li, R.; Cai, M.; Sun, X. Atomic layer deposition of solid-state electrolyte coated cathode materials with superior high-voltage cycling behavior for lithium ion battery application. *Energy Environ. Sci.* **2014**, *7*, 768–778. [CrossRef]